Photonic Crystal Fiber-Based Grating Sensors

56

Changrui Liao, Feng Zhu, and Chupao Lin

Contents

Abstract

Photonic crystal fibers support a powerful platform for the development of novel fiber devices. Combined with fiber grating, which is one of the most important fiber sensor configurations, the photonic crystal fibers exhibit extraordinary superiority in fiber sensing applications. In this chapter, we summarized the recent research works in the field of photonic crystal fiber - based fiber Bragg grating and long period grating and their sensing applications.

Introduction

Since the first publication by Knight et al. (1996) on photonic crystal fiber (PCF) (Knight et al. 1996), the optical fiber community has been continuously worked around these new fibers. A commonly classification of PCF divides into two main categories: index-guiding PCF (IG-PCF) and photonic-bandgap PCF (PBF). The

C. Liao (✉) · F. Zhu · C. Lin
College of Optoelectronic Engineering, Shenzhen University, Shenzhen, China
e-mail: cliao@szu.edu.cn; 2151190226@email.szu.edu.cn; linchupao2016@email.szu.edu.cn

G.-D. Peng (ed.), *Handbook of Optical Fibers*,
https://doi.org/10.1007/978-981-10-7087-7_12

IG-PCF usually contains a solid core, which is surrounded by a microstructured cladding. As a result of the presence of air holes, the effective refractive index of the cladding is smaller than that of the core, and light is guided along the core by the mechanism of total internal reflection. The PBF usually has a hollow core, and the light guidance mechanism is the result of the presence of photonic bandgap in the cladding region for a specific range of wavelengths. By adjusting the size and location of the cladding holes or the core diameter, the fiber transmission spectrum, mode shape, nonlinearity, dispersion, and birefringence can be tuned.

Photonic Crystal Fiber-Based Fiber Bragg Grating (FBG)

Index-Guiding Photonic Crystal Fiber-Based FBG Sensors

The First FBG Fabricated in IG-PCF

FBGs have been extensively investigated as sensing elements in single-mode fibers. The first demonstration of FBG in IG-PCF was made in Bell Labs in 1999 (Eggleton et al. 1999). The employed PCF consists of a Ge-doped core with radius of $\sim$1 μm and $\Delta = (n_{core} - n_{clad})/n_{core} \sim 0.5\%$, where n_{core} and n_{clad} are the refractive index of core and silica cladding. The fiber is loaded with deuterium to enhance the photosensitivity of the core and then exposed through phase mask from a dye laser. Transmission spectrum of IG-FBG is shown in Fig. 1, where some resonant dips from right to left are corresponding to the reflection of core mode and high-order modes.

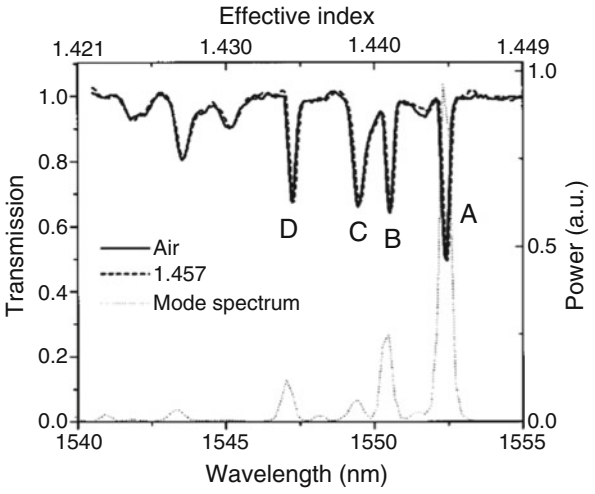

Fig. 1 Transmission spectrum of the FBG in IG-PCF (Eggleton et al. 1999)

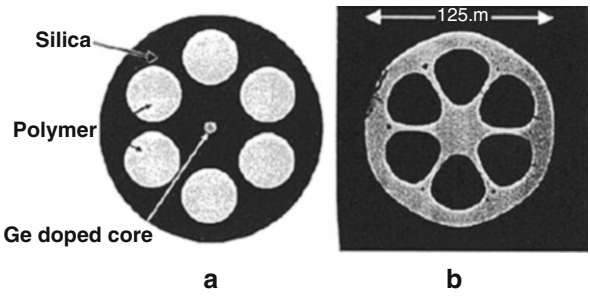

Fig. 2 (**a**) Cross section of the hybrid polymer-silica PCF. (**b**) Optical microscope image of real cross section before polymer infusion (Westbrook et al. 2000)

Temperature Sensing by Use of the FBG in Hybrid Polymer-Silica PCF

The holes in the cladding of IG-PCF allow the design of a wide range of guided-mode properties, which result in unique spectral characteristics of fiber gratings. In 2000, the FBG has been inscribed in a hybrid polymer-silica PCF, which is schematically shown in Fig. 2 (Westbrook et al. 2000). In this PCF, six holes with a diameter of ~40 μm form a hexagonal ring around the central silica region with a diameter of ~32 μm. Ge-doped core with a diameter of ~8 μm and Δ ~0.35% is in the center of the fiber. The fiber is deuterium loaded, and then the FBG is inscribed into the core by scanning exposure through a phase mask with 242-nm dye laser. Then, an acrylate-based polymer with similar refractive index of silica is filled into the air holes and UV cured to form a hybrid waveguide at the grating. The cladding spectrum will be changed with temperature due to the strong temperature dependence of the polymer refractive index.

Temperature Stability of the FBG in All-Silica IG-PCF

FBG inscription in SMFs usually relies on photosensitivity of core dopants (like germanium), and this photosensitivity can be enhanced by hydrogen loading treatment. FBGs in such doped fibers can be inscribed by use of single photon absorption at 242–248 nm using KrF excimer (248 nm) or frequency-doubled argon-ion (244 nm) lasers. However, pure silica is not photosensitive at 244 nm, so alternative grating inscriptions are required for pure silica IG-PCFs. In 2005, the FBG has been firstly inscribed in all-silica PCF with femtosecond laser at 267 nm (Fu et al. 2005). Gratings have been fabricated with a depth of 10 dB and an average of $\Delta n > 4 \times 10^{-4}$. An isochronal annealing has been done to evaluate the stability of the grating, and it is found that the refractive index monotonically decreased as a function of temperature. This decay performance indicates that the grating has an origin related to both defect formation and the compaction mechanism active in fused silica at 193 nm.

Strain Sensing by Use of the FBG in Holey IG-PCF

Han Y.-G et al. have investigated the effect of air-hole size on the strain response of the FBGs inscribed in four different holey fibers with a germanium-doped core and one-layered air holes in silica cladding, as shown in Fig. 3 (Han et al. 2006). The

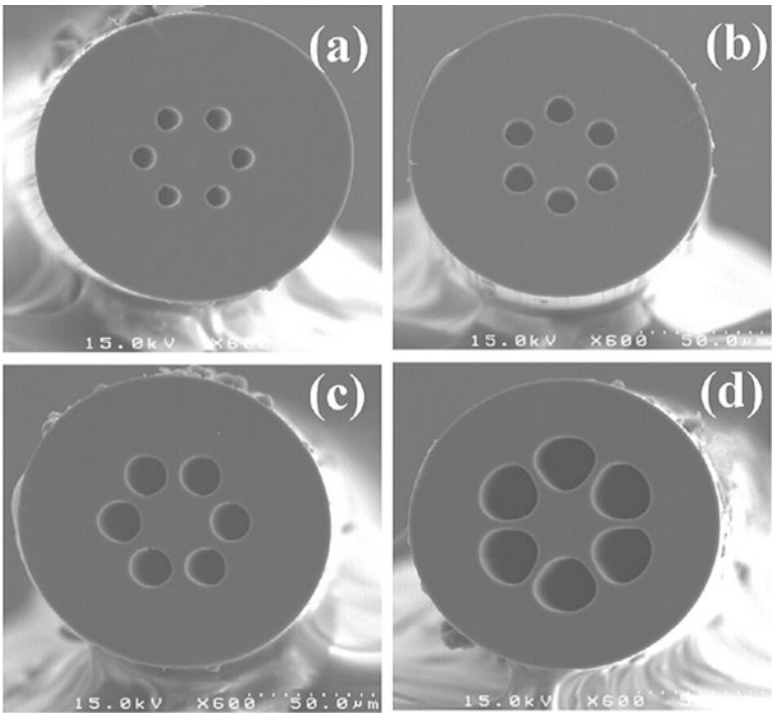

Fig. 3 SEM images of the cross section of four different holey IG-PCFs (Han et al. 2006)

FBGs have been fabricated by use of beam-scanning technique with 244 nm Ar^+ laser, and hydrogen loading treatment is taken to enhance the photosensitivity of the Ge-doped core. After fabricating FBGs, annealing process during 24 h is taken to remove unreacted hydrogen to stabilize the quality of FBGs.

The strain sensitivity of the FBGs in holey fibers corresponding to air-hole size has been experimentally investigated. The strain sensitivity of the FBGs can be written as

$$\frac{\partial \lambda_p}{\partial \varepsilon} = \lambda_p \left(1 - \rho\right) \varepsilon \tag{1}$$

where λp is the center wavelength of the FBG, ρ is the photoelastic coefficient, and ε is the applied strain. Since four types of holey fibers have the different cross-sectional area due to different sizes of air holes, their strain sensitivities become different corresponding to air-hole size. Figure 4 shows the center wavelength shift of FBGs with strain changes, and it can be found that the strain sensitivity is significantly enhanced as air-hole size increased because of small glass volume due to the air holes inside of silica cladding.

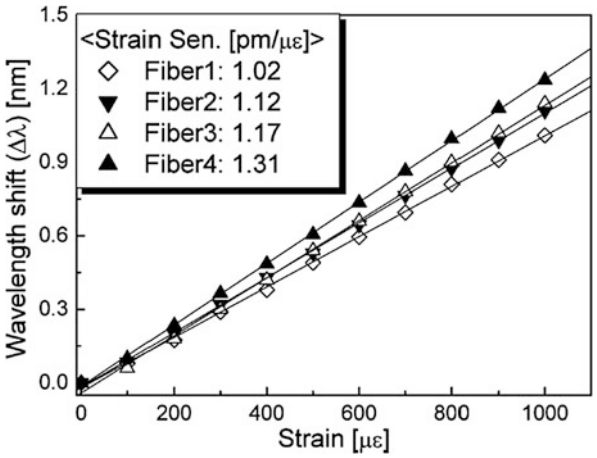

Fig. 4 Strain sensitivity of FBGs fabricated with holey fibers corresponding to air-hole size (Han et al. 2006)

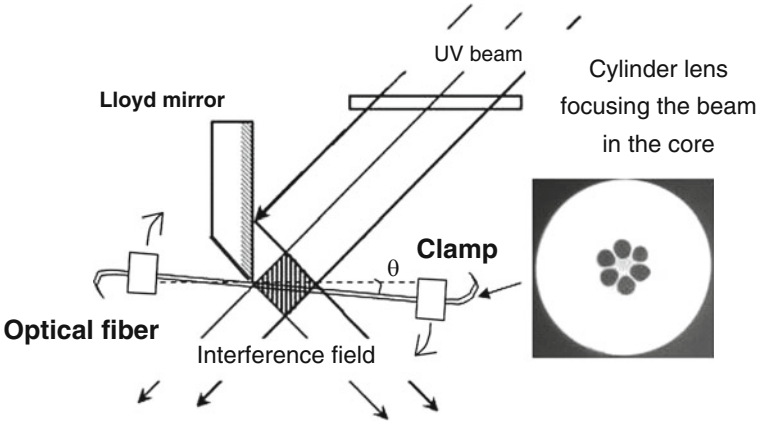

Fig. 5 Lloyd mirror interferometer setup used for tilted FBG inscription (Huy et al. 2006)

Refractive Index Sensing by Use of the FBG in Holey IG-PCF

Huy et al. demonstrated a tilted FBG sensor inscribed in IG-PCF as an optical refractometer (Huy et al. 2006). The employed fiber can be described by a ring of six air holes ($d \sim 15\ \mu m$ and $\Lambda \sim 15.8\ \mu m$), surrounding a noncircular and slightly decentered core of 11 μm in diameter, as shown in the inset of Fig. 5. Such a fiber is multimode in 1.5-μm spectral window. Fibers are required to be hydrogen-loaded to increase the photosensitivity of Ge-doped core. Tilted FBGs are inscribed by use of Lloyd mirror interferometer including a CW frequency-doubled argon laser emitting at 244 nm. The experimental setup is demonstrated in Fig. 5, where the fiber is held straight on between two clamps fixed on a rotary stage and the required angle θ between the fiber axis and the interference fringes pattern is precisely adjusted.

Spectral responses in transmission of tilted FBG inscribed in the six-hole PCF are shown in Fig. 6. For $\theta = 0°$, not only the Bragg resonance but also resonances to

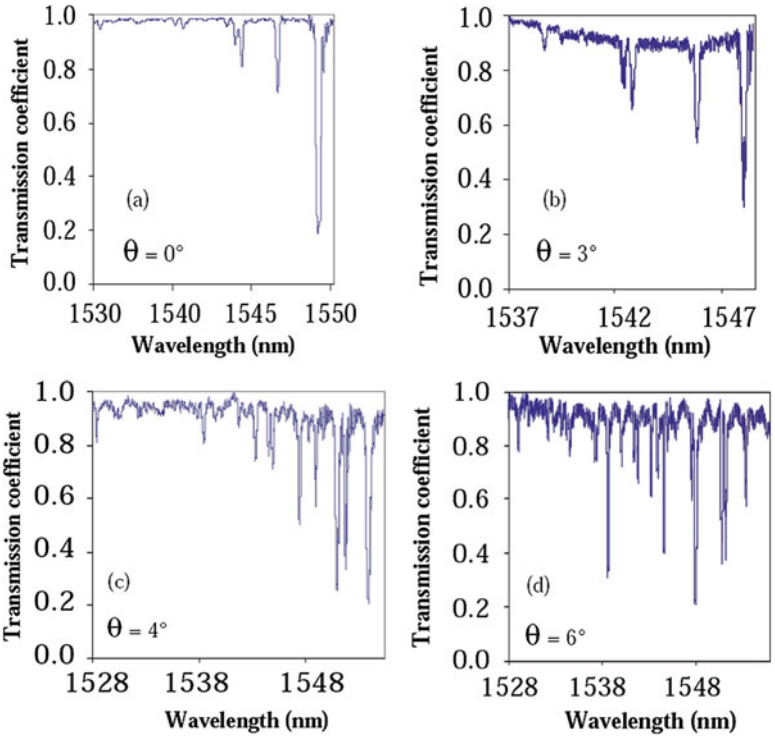

Fig. 6 Transmission spectra of (**a**) non-tilted, (**b**) 3°-tilted, (**c**) 4°-tilted, (**d**) 6°-tilted FBG written in the six-hole PCF (Huy et al. 2006)

higher-order modes can be observed. When θ increases, more and more transmission dips are distinguishable on the spectrum, indicating that more and more modes are involved in the coupling process.

Refractive index response experiment consists in introducing several calibrated refractive index liquids into the holes of the PCF and to determine the consequences on the spectral resonances of a tilted FBG. These liquids are successively inserted into the fiber holes of a unique fiber section, without removing the previous one. The spectral resonances experience a red shift, when a given liquid reaches the tilted FBG (see Fig. 7). The insertion of any liquid modifies the interaction with the evanescent field of the guided mode and hence the effective index. The effective index of the guided modes increases together with the refractive index of the inserted liquid.

Transversal Load Sensing by Use of the FBG in Hi-Bi PCF

T. Geernaert et al. presented an FBG written in Hi-Bi PCF to monitor stress inside a composite material (Geernaert et al. 2009). The microstructure of the PCF consists of three rows of air holes and a central Ge-doped core, as shown in Fig. 8. The

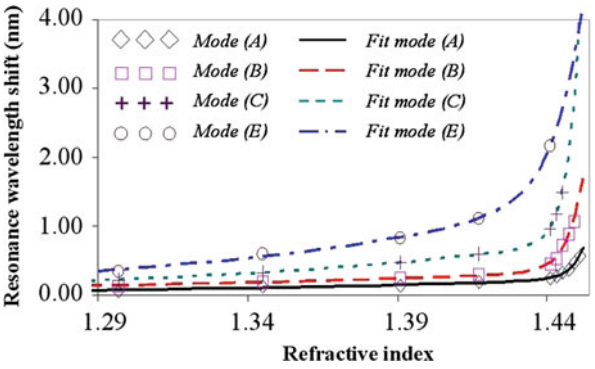

Fig. 7 Wavelength shift of the first four resonances versus the refractive index of the liquid (Huy et al. 2006)

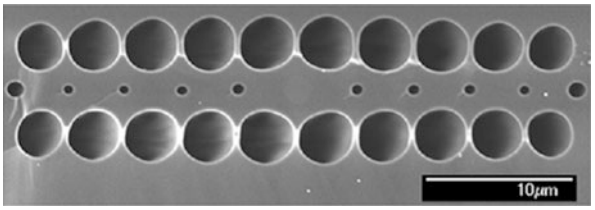

Fig. 8 SEM image of the cross section of the microstructure (Geernaert et al. 2009)

diameter of the PCF is 125 μm and the Ge-doped core is circular, and the lattice constant of the microstructure is 3.9 μm. The phase modal birefringence of this PCF is measured to be $\sim 8 \times 10^{-4}$ at 1550 nm. Since the PCF is birefringent, unpolarized light that is launched into the fiber yields two Bragg peaks, one for each orthogonally polarized mode propagating in the fiber. The peak separation is related to the phase modal birefringence by

$$\Delta\lambda = \lambda_{B2} - \lambda_{B1} = 2 \times B \times \Lambda \tag{2}$$

where Λ is the grating period in the core.

In the transversal load test, an 8-mm-long FBG is embedded between two carbon fiber reinforced epoxy laminates. The stress on the sample is continuously increased from 0 up to 4 MPa. The Bragg peak separation changes at a constant rate of 15.3 pm/MPa. The original Bragg peak separation of ∼1 nm is large enough to guarantee that the two Bragg peaks remain well separated and can be detected, as shown in Fig. 9.

Gas Pressure Sensing by Use of the FBG in Grapefruit PCF

C. Wu et al. demonstrated FBGs written in grapefruit PCFs, which are used for pressure sensing (Wu et al. 2010). Figure 10 shows the cross sections of the two employed grapefruit PCFs. Both PCFs have outside diameter of 125 μm and core diameter of 8 μm. The large-hole PCF has hole diameter of 33.8 μm in radial direction. The small-hole PCF has hole diameter of 17 μm and hole pitch

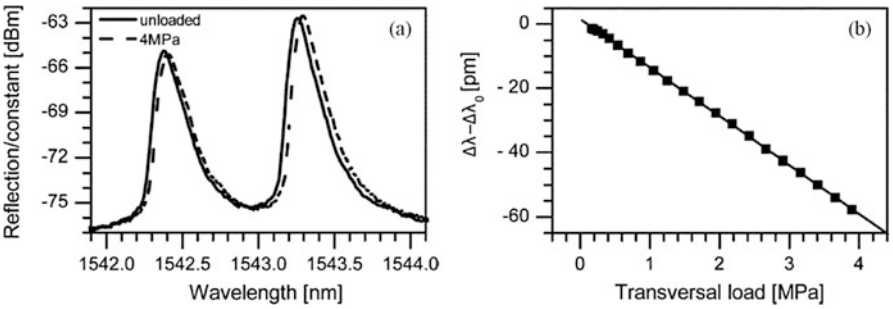

Fig. 9 (**a**) FBG reflection spectrum of the embedded FBG in the Hi-Bi PCF with transversally load and unloaded. (**b**) Variation of the Bragg peak separation versus transversal stress (Geernaert et al. 2009)

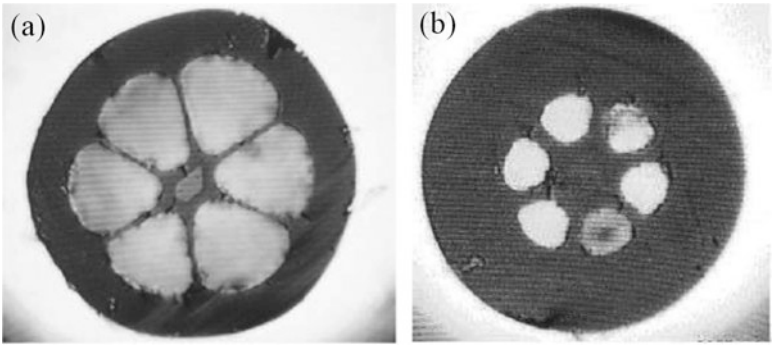

Fig. 10 Cross sections of (**a**) large-hole grapefruit PCF and (**b**) small-hole grapefruit PCF (Wu et al. 2010)

of 25.4 μm. The core of both PCFs is doped with germanium to enhance the photosensitivity.

FBGs have been inscribed in the grapefruit PCFs by use of 193-nm excimer laser and a phase mask. To characterize their response to pressure, the FBGs are located in a pressure chamber, and the pressure is changed from 0 to 25 MPa in a step of 2.5 MPa. Experimental results of wavelength shift as a function of pressure in two PCFs are shown in Fig. 11. It is found that the FBGs in grapefruit PCF show much higher pressure sensitivity than normal FBG.

Photonic-Bandgap Photonic Crystal Fiber-Based FBG Sensors

Bend Sensing Based on the FBG in All-Solid PBF

L. Jin et al. presented the FBGs inscribed into the all-solid PBF by forming a longitudinal periodic index modulation over the high-index rod lattice in the cladding (Jin et al. 2007). In the fiber, a Ge-doped high-index rod lattice of six layers

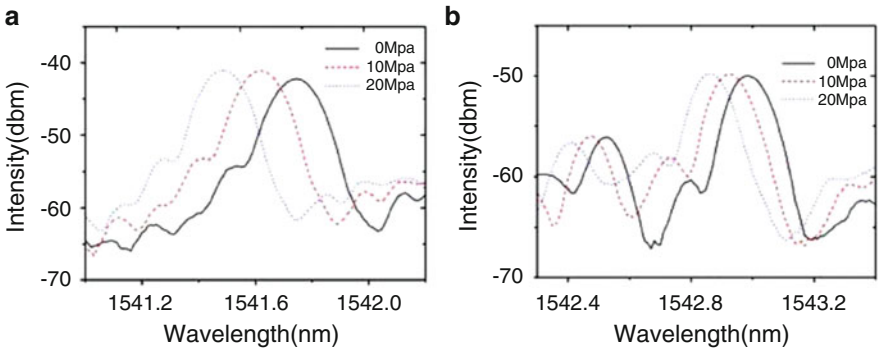

Fig. 11 Reflection spectra at different pressure of (**a**) large-hole PCF and (**b**) small-hole PCF (Wu et al. 2010)

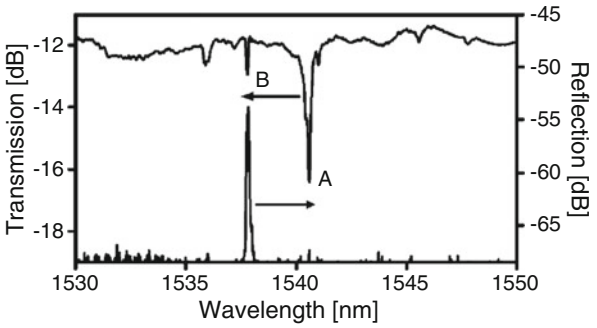

Fig. 12 Transmission and reflection spectra of the FBG in all-solid PBF (Jin et al. 2007)

is embedded in pure silica background (the index difference is 1%), and the core is formed by omitting a single rod. The pitch Λ of the high-index rods is 11 μm, and the nominal ratio of the diameter of the raised-index rods to the pitch is $d/\Lambda = 0.4$. The outer diameter is $\sim$200 μm. The Ge-doped rod lattice in the cladding enables index modulation by UV light.

A length of PBF is firstly spliced to SMFs and then loaded in a hydrogen atmosphere at 100 atm, 100 °C for 48 h to enhance its photosensitivity. The PBF is then exposed by 248-nm KrF excimer laser at a repetition rate of 5 Hz for 15 min. The grating period is 532.5 nm, and the grating length is 1.3 cm. Figure 12 shows the transmission and reflection spectra of the FBG, from which peaks A (1540.58 nm, 4.4 dB) and B (1537.8 nm, 1.1 dB) are observed. However, only dip B finds its corresponding reflective peak in the reflection spectrum because the guided mode has the largest overlap with SMF among all the modes.

Figure 13a shows the transmission spectrum of the offset launched FBG. The fluctuation of the spectral background is caused by complicated couplings between the high-index rods and the defect core. No noticeable changes in the resonance depths of dips A and B are observed when the lateral offset is applied. Figure 13b

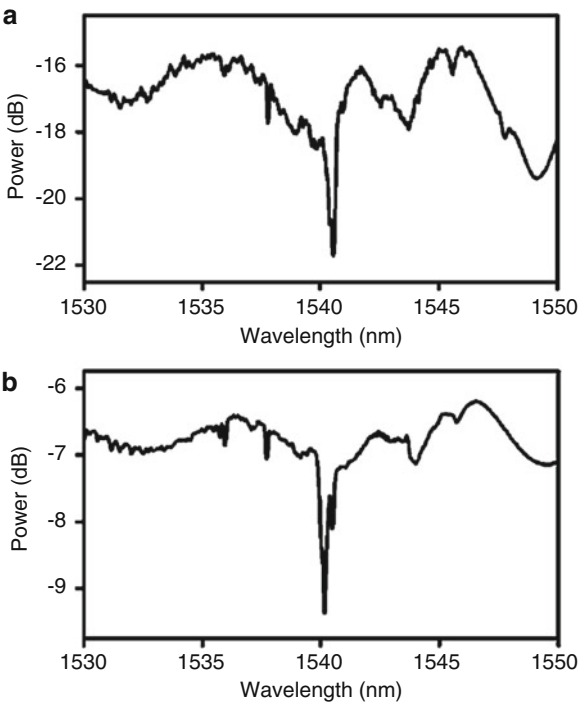

Fig. 13 (**a**) Transmission spectrum of the FBG with lateral offset between the launched SMF and the FBG. (**b**) Split of the super-mode resonance peak A when the FBG is bent (Jin et al. 2007)

shows the splits of the super-mode resonance peak A. The two separated peaks correspond to backward rod modes in stretched and compressed rods and the wavelength separation increases with curvature due to enhanced index gradient over the fiber. The FBG can be potentially applied for sensing directional bend.

High-Temperature Sensing by Use of the FBG in All-Solid PBF

Y. Li et al. reported the FBGs written in all-solid PBF by use of femtosecond laser through a phase mask (Li et al. 2009). The fiber is exposed to 800-nm 120-fs laser pulses from a Ti/sapphire amplifier with the repetition rate of 1 kHz and the 1/e Gaussian beam radius of 2 mm. The laser beam is focused using a cylindrical lens before passing through phase mask to illuminate the PBF. By carefully adjusting the focal line to be located in the fiber core, the grating is successfully formed due to refractive index modulation in the core, induced by multiphoton absorption. The transmission and reflection spectra are shown in Fig. 14.

Morphology of femtosecond laser-induced grating in all-solid PBF is shown in Fig. 15. The grating lines are located in the fiber core area as shown in Fig. 15a, where the laser incident direction is plotted. The influence area of the femtosecond pulses along the beam propagation direction was shown in Fig. 15b, where the cross section of the fiber is cleaved at the center of the grating. It can be observed that except for the all-silica core area, the Ge-doped rods are not affected by the laser pulses and remained unchanged.

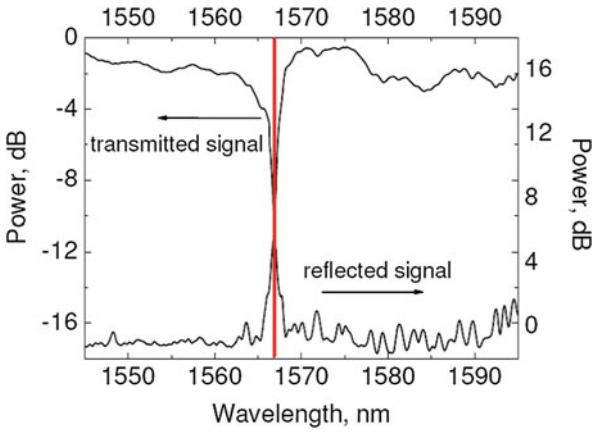

Fig. 14 Transmission and reflection spectra of the FBG in all-solid PBF (Li et al. 2009)

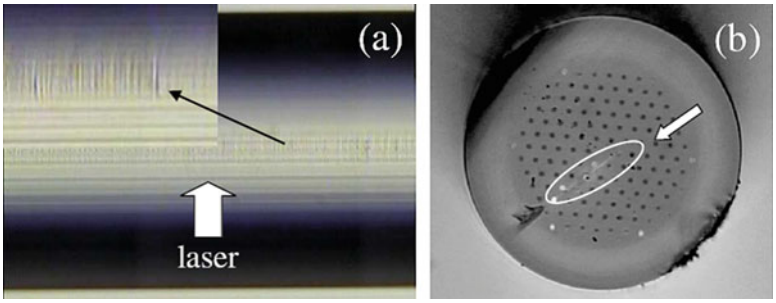

Fig. 15 Optical microscope images of the grating morphology in the (**a**) longitudinal and (**b**) the cross section of the fiber (Li et al. 2009)

The annealing characteristic of the FBG in all-solid PBF is shown in Fig. 16. The gratings are more thermally stable when compared with UV-laser-induced samples. The gratings are almost unaffected by the thermal exposure up to 700 °C, following which a slowly decay occurred at the elevated temperatures. The temperature corresponding to the 50% decrease in the normalized refractive index change is 900 °C, instead of 650 °C for the UV-laser-induced gratings in H2-free fibers, even higher than that of the type I femtosecond laser-induced gratings in Ge-doped SMF-28 fibers.

Photonic Crystal Fiber-Based Long Period Grating (LPG)

Index-Guiding Photonic Crystal Fiber-Based LPG Sensors

Long-period fiber grating (LPG) is another useful structure that can be written in PCF. Many different fabrication methods have been reported, and these fiber gratings have been used in diversified sensing applications.

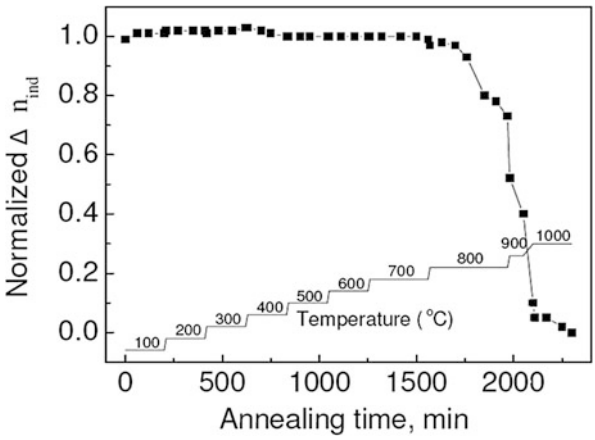

Fig. 16 Thermal degradation of the FBG written in all-solid PBF, with elapsed time over various temperature ranges (Li et al. 2009)

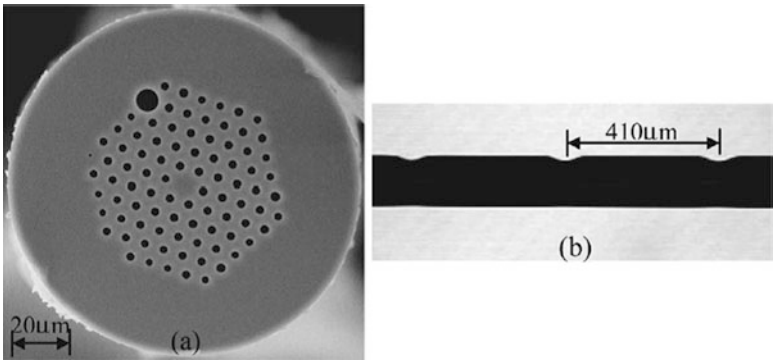

Fig. 17 (**a**) SEM image of the cross section of the PCF. (**b**) CCD photograph of the LPG with periodic grooves (Wang et al. 2006)

Strain Sensing by Use of the Carved LPG in IG-PCF

Y. P. Wang et al. demonstrated a PCF-based LPFG sensor with a high strain sensitivity of -7.6 pm/$\mu\varepsilon$, which is fabricated by use of focused CO_2 laser beam to carve periodic grooves on a large mode-area PCF (Wang et al. 2006). The SEM image of the cross section of the PCF employed is illustrated in Fig. 17b, where the PCF has a center-to-center distance between the air holes of 6.1 μm and an average air-hole diameter of $d = 1.8$ μm. The holes are arranged in a hexagonal pattern, which has a diameter of 65 μm.

The periodic grooves carved by CO_2 laser irradiation is shown in Fig. 17b. Such grooves can induce periodic refractive index modulations along the fiber axis due to the photoelastic effect, thus creating an LPFG. The groove's depth, which indicates the efficiency of CO_2 laser heating and the refractive index modulation, depends

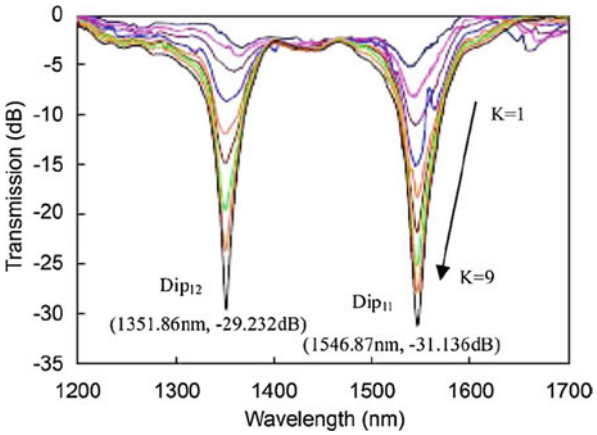

Fig. 18 Transmission spectral evolution of the LPG with the number, K, of scanning cycles being increased from 1 to 9, where $N = 40$ and $M = 5$ (Wang et al. 2006)

on the fabrication parameters. In the experiments, the diameter of the focused CO_2 laser beam spot is $\sim$35 μm.

Figure 18 shows the transmission spectral evolution of the LPG with asymmetric periodic grooves, where a low insertion loss of $\sim$2 dB and two attenuation dips (Dip11 and Dip12) are produced after nine scanning cycles, where the resonant wavelengths and the peak transmission attenuations of Dip11 and Dip12 are $\lambda 11 = 1546.87$ nm, $A11 = -31.136$ dB, $\lambda 12 = 1351.86$ nm, and $A12 = -29.232$ dB, respectively.

Figure 19 shows the schematic diagram of the carved LPG before and after a stretching force. The refractive index modulation in the carved LPFG that is stretched can be expressed as $\Delta n = \Delta n_{residual} + \Delta n_{groove} + \Delta n_{stretch}$, where $\Delta n_{residual}$ is the initial refractive index perturbation induced by the residual stress relaxation resulting from the high local temperature, which is similar to the case of the CO_2-laser-induced LPGs without periodic grooves; Δn_{groove} is the initial refractive index perturbation induced by the periodic grooves on the fiber; $\Delta n_{stretch}$ is the refractive index perturbation induced by the stretching force and can be expressed as $\Delta n_{stretch} = \Delta n_{strain} + \Delta n_{microbend}$, where Δn_{strain} is the refractive index perturbation induced by the difference between the stretch-induced tensile strains in the grooved and ungrooved regions via the photoelastic effect; $\Delta n_{microbend}$ is the refractive index perturbation induced by the stretch-induced microbends and this stretch-induced microbends effectively enhance refractive index modulation.

Tensile strain responses of two LPGs with and without periodic grooves have been compared. With the increase of the tensile strain, the resonant wavelengths of the LPG with periodic grooves shift rapidly toward the shorter wavelength and a good linearity is observed, whereas that of LPG without periodic grooves shifts slowly toward the shorter wavelength. The strain sensitivity of resonant wavelength of the LPGs written by CO_2 laser in the same fiber is increased by 25 times by means of carving periodic grooves on one side of the fiber.

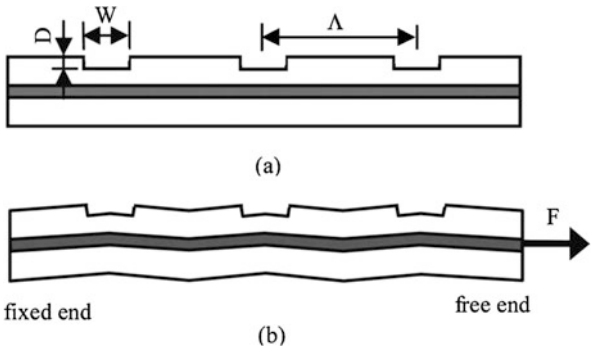

Fig. 19 Schematic of the CO_2-laser-carved LPFG (**a**) before and (**b**) after a stretching force (Wang et al. 2006)

Bend Sensing by Use of the LPG in IG-PCF

L. Jin et al. presented a directional bend sensor based on an LPG formed by introducing periodic grooves along one side of a PCF with a focused CO_2 laser beam (Jin et al. 2009). The fiber used for LPG fabrication is the crystal fiber's LMA-10 PCF, as shown in Fig. 20a. A focused CO_2 laser beam is controlled by a computer and scanned transversely across the fiber with a certain longitudinal period over a length of fiber, and the scanning may be repeated for a number of scanning cycles to produce LPGs with required strength of resonant coupling. The transmission spectrums and polarization-dependent loss (PDL) profiles of the LPG are shown in Fig. 20d, and the notches on one side of fiber surface and air-hole collapse and deformation are shown in Fig. 20b. The width and depth of the individual notches are estimated to be 70 and 12 μm, as shown in Fig. 20c.

Figure 21a shows the measured mode field of the LPG at the resonance wavelength under bend-free condition. The observed highly asymmetric mode intensity profile is a result of both structural change and asymmetric index modulation. The cladding mode intensity distribution around the core region is not easy to observe due to the existence of the uncoupled core mode; however, the shift of the cladding mode power to the unchanged side of the cladding is obvious. Figure 21b shows the measured bending response of LPG. The LPG has a directional bending response toward and against the notches and a relatively good linear response. The overall sensitivity is 2.26 nm/m^{-1} within the range of $-5 \sim +5$ m^{-1}. The directional response mainly arises from the structural modifications in the PCF cladding, although the asymmetrical glass refractive-index modulation may also play a role. The good linear response and the simple fabrication process make the proposed sensor a suitable candidate for low-cost structural shape sensing in harsh environments.

Gas Pressure Sensing by Use of an Inflated LPG in IG-PCF

X. Y. Zhong et al. demonstrated the inscription of an inflated LPG (I-LPG) in a PCF by means of the pressure-assisted CO_2 laser beam-scanning technique to inflate periodically air holes along the fiber axis (Zhong et al. 2015). Figure 22 illustrates the detailed process for fabricating an I-LPG. First, as shown in Fig. 22a, an end of

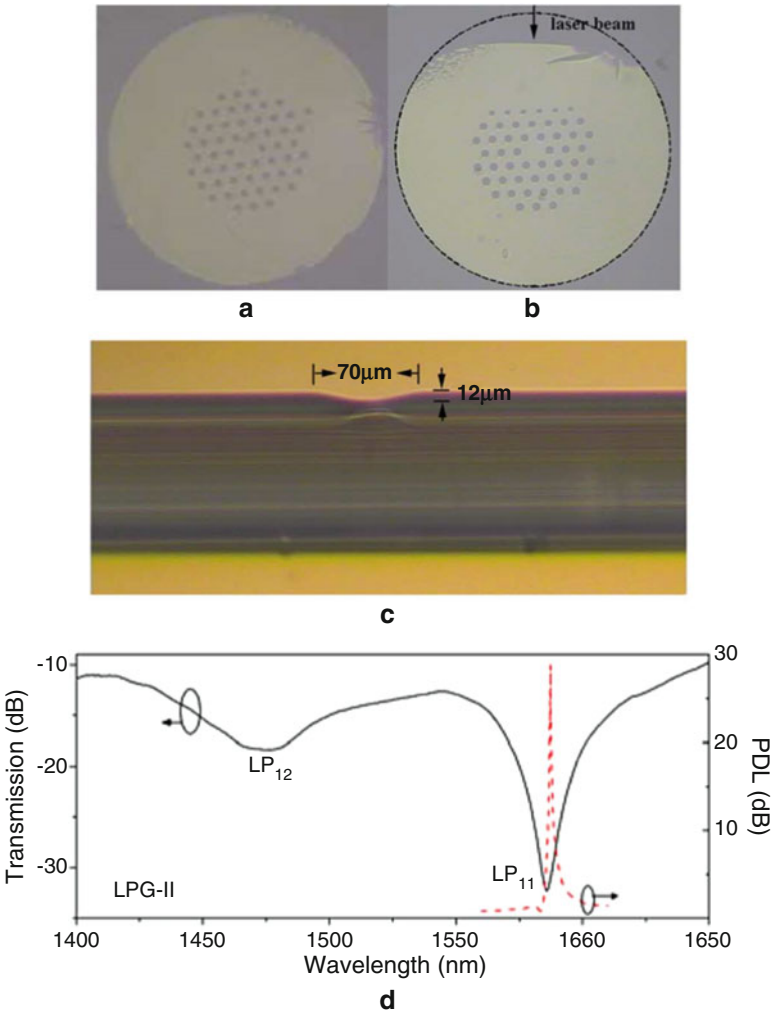

Fig. 20 Microscopic photographs of the PCF cross section (**a**) before and (**b**) after CO_2 laser irradiation. Air-hole collapse/deformation in the fiber cladding and the notch on the fiber surface is clearly observable in (**b**) and (**c**). The transmission spectrums and measured PDL profiles of the LPG in (**d**) (Jin et al. 2009)

a silica tube was spliced with a large-mode-area pure silica PCF (NKT ESM-12). Second, as shown in Fig. 22b, another end of the silica tube was cleaved to shorten its length to be about 80 μm to observe whether the air holes of the PCF end are open or not by use of a microscope. Third, as shown in Fig. 22c, the cleaved end of the silica tube was spliced with another SMF, thus achieving an air cavity with a length of 80 μm. And then a micro-channel (50*40 μm) was drilled through the sidewall of the silica tube by use of a femtosecond laser so that air pressure can access from

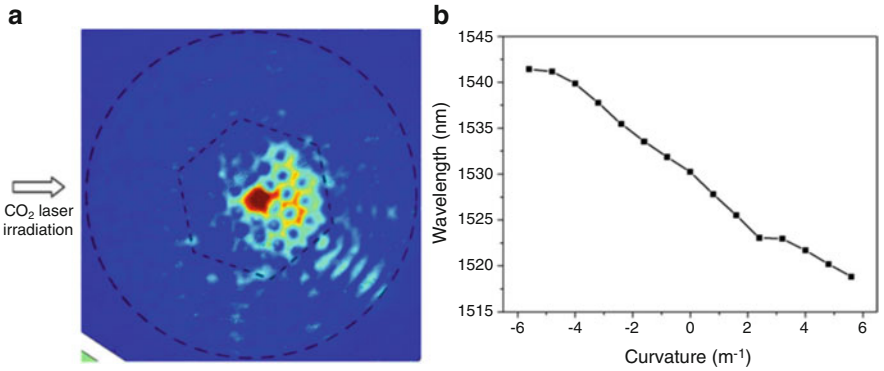

Fig. 21 (**a**) Measured near-field intensity profile at the output end of LPG at the resonance wavelength when the fiber is bend-free. (**b**) Measured bend response of the LPG. The measurement result shows a directional bending response with good linearity (Jin et al. 2009)

the silica tube into the air holes of the PCF. Fourth, as shown in Fig. 22d, the silica tube with a channel was placed into a gas chamber and sealed by use of strong glue. Then air with a pressure of ~1.5 MPa accessed the holes of the PCF via the gas chamber by use of a high-pressure air pump. Finally, as shown in Fig. 22e, f, the PCF was periodically heated along the fiber axis by use of a focused CO_2 laser beam. As a result, the holes of the PCF inflated periodically along the fiber axis due to high-pressure air and the CO_2-laser-induced high temperature.

In Fig. 23a, air holes of a PCF employed with a diameter of 3.3 μm are arranged in a hexagonal pattern with a pitch of 7.4 μm. The core and cladding diameters of the PCF are 10.4 and 125 μm, respectively. In Fig. 2b, asymmetric inflations of air holes were clearly created in the PCF along the fiber axis, resulting from the single-side irradiation of the focused CO_2 laser beam. Compared with the PCF diameter of 125 μm, the inflated region of the PCF has a diameter of 130 μm along the CO_2 laser irradiation direction. Uneven expansion of the air holes illustrated in Fig. 23b may be due to the inhomogeneity of the air holes in the PCF.

Figure 24 shows the transmission spectrum evolution of CO_2 laser-inscribed LPG with periodic inflations with scanning cycles increasing from 1 to 10. It can be seen from this figure that there is a low insertion loss of ~1 dB, and two attenuation dips (Dip11 and Dip12) are induced after ten scanning cycles.

Gas pressure response of the I-LPFG was measured with the gas pressure being increased from 0 to 10 MPa with a step of 1 MPa. As shown in Fig. 25, the resonant wavelength of I-LPG is shifted toward longer wavelength with a sensitivity of 1.68 nm/Mpa. For I-LPG, the silica wall within the inflated region is thinned due to the inflation of air holes in the PCF. As a result, in the case of a high gas pressure, physical deformations easily occur within the inflated region of the I-LPG, which changes the effective refractive index difference due to elasto-optical effect and induces a resonant wavelength shift. Thus periodic inflations in the I-LPG greatly enhance the pressure sensitivity of the grating.

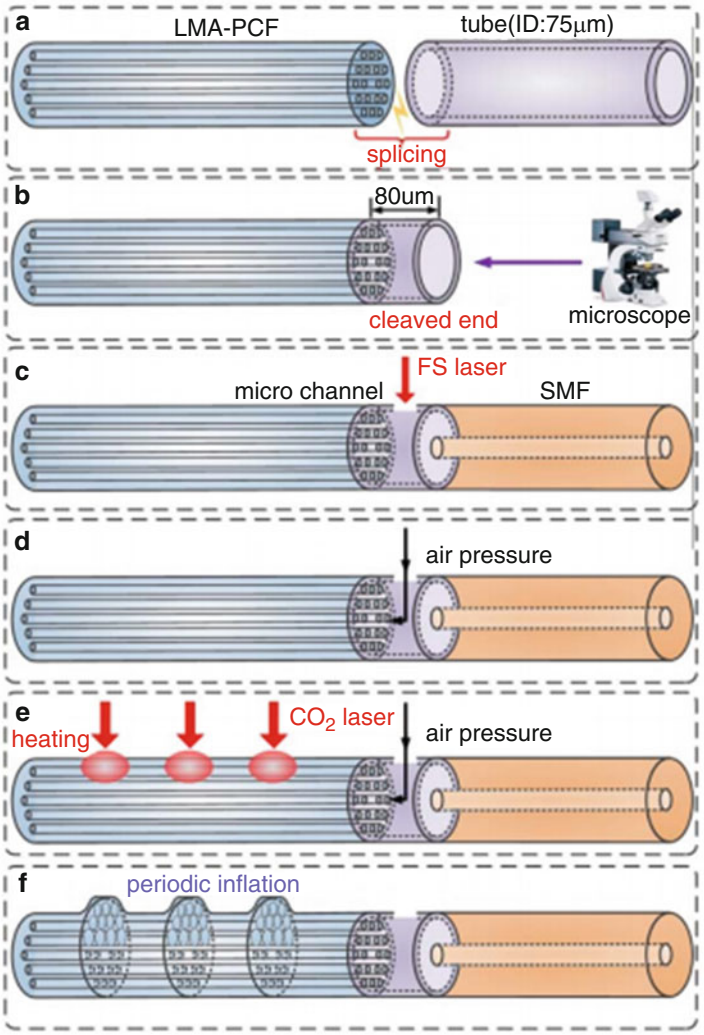

Fig. 22 Schematic diagram for fabricating an I-LPG (Zhong et al. 2015)

Refractive Index Sensing by Use of the Mechanical LPG in PCF

X Yu. et al. realized a refractive index sensor with the measurand infiltrated into the holes of single-mode PCF (Yu et al. 2008). The SEM image of an endlessly single-mode PCF Crystal-Fiber A/S) used for the experiment is shown in Fig. 26. It has a pitch size of 8 μm and air-hole diameter of 3.68 μm. The diameter of holey region is ∼60 μm, and the outside diameter of fiber is 125 μm. A series of calibrated refractive index liquids are infiltrated into the fiber based on the capillary effect with a syringe pump.

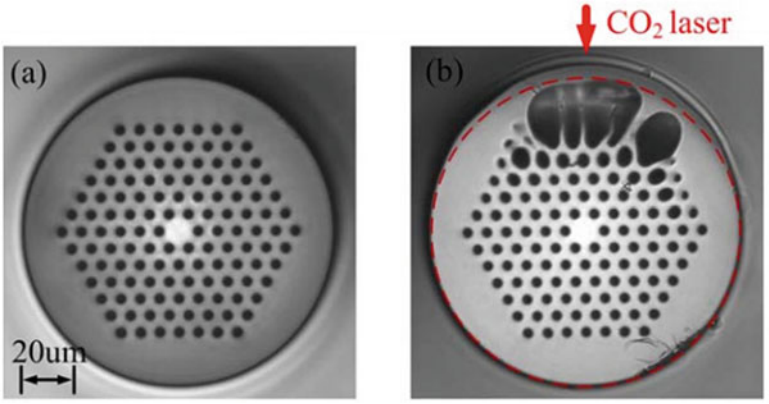

Fig. 23 Microscope image of the cross section of the PCF (**a**) before and (**b**) after CO_2 laser irradiation (Zhong et al. 2015)

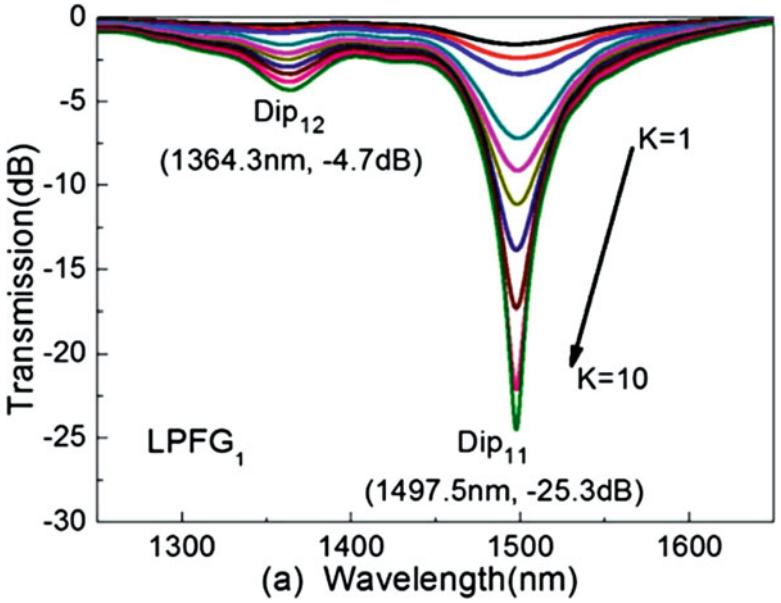

Fig. 24 Transmission spectral evolution of CO_2 laser-inscribed I-LPG with periodic inflations while scanning cycles increase (Zhong et al. 2015)

The LPG is fabricated by applying a transverse force on the section of PCF by a periodically grooved plate as shown in Fig. 26. The fixture is mechanically polished with rectangular grooves of period 600 μm. The length, width, and thickness of the grooved plate were 50, 20, and 5 mm, respectively. The transverse force is manually controlled by a stress gauge with 25 N to achieve a transmission dip ∼15 dB. The grating period is not varied with the increase of the applied force since the grooved

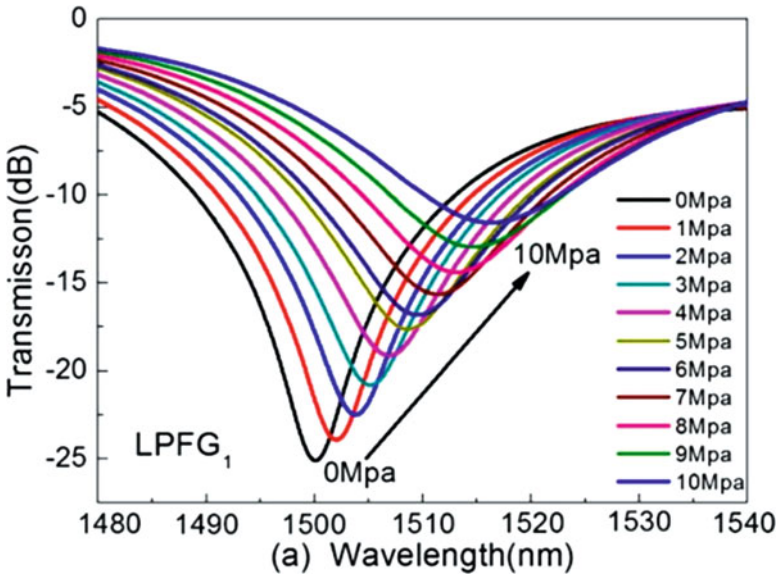

Fig. 25 Transmission spectral evolution of I-LPG while the gas pressure increases from 0 to 10 MPa (Zhong et al. 2015)

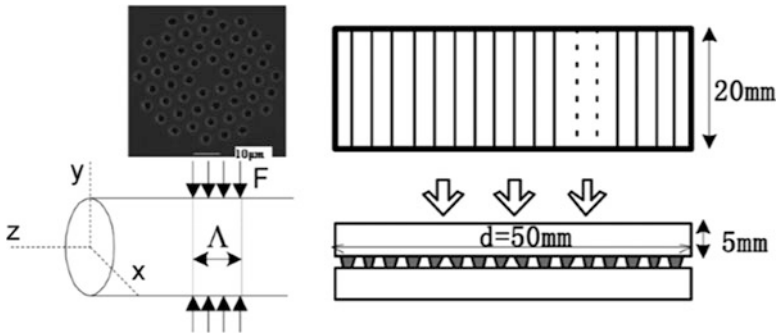

Fig. 26 SEM image of the PCF and grooved fixture and coordinate system for the fiber showing the applied external force (Yu et al. 2008)

plate is placed on top of the flat surface. Thus, the photoelastic effect induces index variations dominating the resonance position.

Figure 27a shows the transmission spectra of the PCF-based mechanical LPG with different infiltration index of 1.32, 1.36, and 1.38. Several measured transmission spectra ∼1420 nm are achieved with different infiltration refractive index. The resonance wavelength is shifted from 1429.50 to 1414.80 nm when the infiltrated index oil changes from 1.32 to 1.38. The refractive index resolution can be obtained from the shift of transmission dip as shown in Fig. 27b. The resonance wavelength shift is 17.1 nm with a refractive index change of 0.07. A linear fitting to the

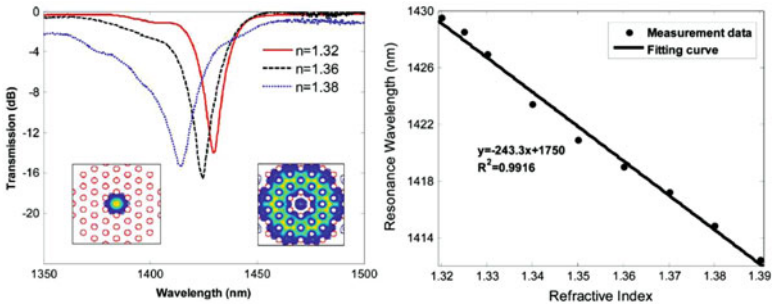

Fig. 27 (**a**) Transmission spectra of the PCF-based mechanical LPG with different infiltration index of 1.32, 1.36, and 1.38. (**b**) Measurement results and fitting curve for the resonance wavelength shift versus the infiltrated refractive index (Yu et al. 2008)

experimental data gives a wavelength-RI sensitivity of 2.4 pm for 1×10^{-5} change in the index proportionally.

Biochemical Sensing by Use of the LPG in PCF

L. Rindorf et al. reported the first label-free technique for detection of biomolecules using a PCF-based LPG (Rindorf et al. 2006). The LPG is inscribed by use of CO_2 laser scanning on the PCF (LMA10), which has a pitch of 7.2 μm and a relative (absolute) hole size of d/L = 0.47. The pitch of the PCF-LPG is 700 μm. The number of grating periods is chosen to be 26 making the length of grating 18.2 mm. The length of the fiber with the PCF-LPG in the middle is 30 cm in total. To introduce the solutions into the holes of the PCF, one end of the PCF is inserted into a pressure chamber.

As shown in Fig. 28, poly-L-lysine is used to immobilize negatively charged molecules such as DNA to a solid support. Poly-L-lysine has positively charged amino groups that can bind to the negatively charged silica surface through an ionic binding. DNA, on the other hand, has negatively charged phosphate groups in its backbone, and may thus be immobilized in a monolayer onto the poly-L-lysine, but cannot bind directly onto the silica.

Figure 29 shows the result of biochemical sensing. The resonant wavelength of the grating with air inside the holes is 753.6 nm. The introduction of the PBS into the holes caused the resonant wavelength to shift to 842.5 nm, giving a total shift of 88.9 nm. The immobilization of poly-L-lysine shifts the resonant wavelength to 849.2 nm, a shift of 6.7 nm. Finally, the DNA shifts the resonant wavelength to 851.4 nm, a shift of 2.3 nm.

Photonic-Bandgap Photonic Crystal Fiber-Based LPG Sensors

The First LPG in Air-Core PBF

In 2008, Y. P. Wang et al. reported the first LPG written in air-core PBF by use of CO_2 laser pulses to periodically modify the size, shape, and distribution of air holes

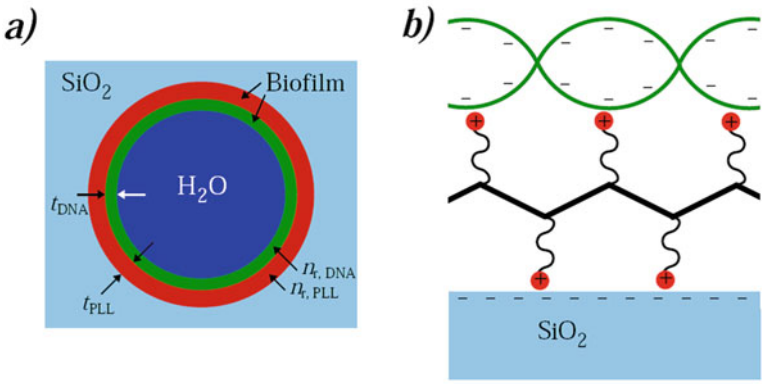

Fig. 28 (**a**) A hole of a photonic crystal fiber. The side is coated with poly-L-lysine and DNA in monolayers of various thickness (t_{DNA} and t_{PLL}) and refractive indices ($n_{r,DNA}$ and $n_{r,PLL}$). The thickness of the biofilms is vastly exaggerated compared to the hole diameter. (**b**) The molecular structure of poly-L-lysine (*red* and *black*) with positive charges immobilized onto the negatively charged silica surface (SiO_2). The negatively charged DNA (*green*) is immobilized on the poly-L-lysine (Rindorf et al. 2006)

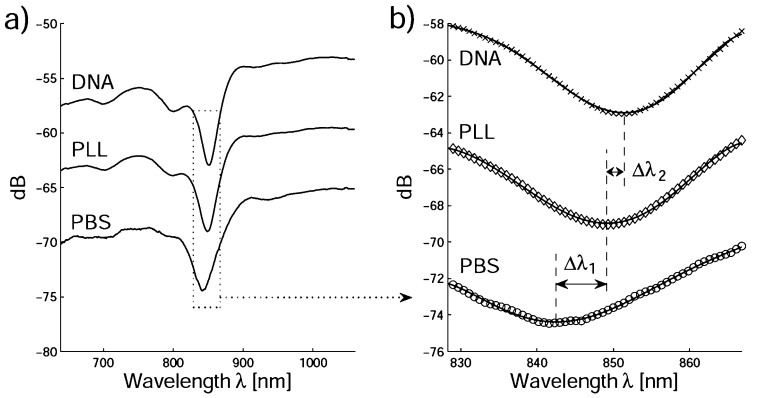

Fig. 29 Transmission spectra for PBS, poly-L-lysine (PLL), and DNA (Rindorf et al. 2006)

in the microstructured cladding (Wang et al. 2008). The fiber used is Crystal-Fiber's HC-1500-02 PBFs with a cross section shown in Fig. 30a. These high frequency, short duration, and CO_2 laser pulses hit repeatedly on one side of the PBF and induce a local high temperature, causing ablation of glass on the surface and change of shapes, sizes, locations, and even complete collapse of some of the air holes in the cladding, as shown in Fig. 30b. This results in a notch being created on the surface of the fiber, as shown in Fig. 30c. Figure 30d shows the measured transmitted spectrum of a 40-period LPG made by the above process. The 3 dB bandwidth is ~5.6 nm, which is much narrower than that of the LPGs in conventional SMFs. The insertion

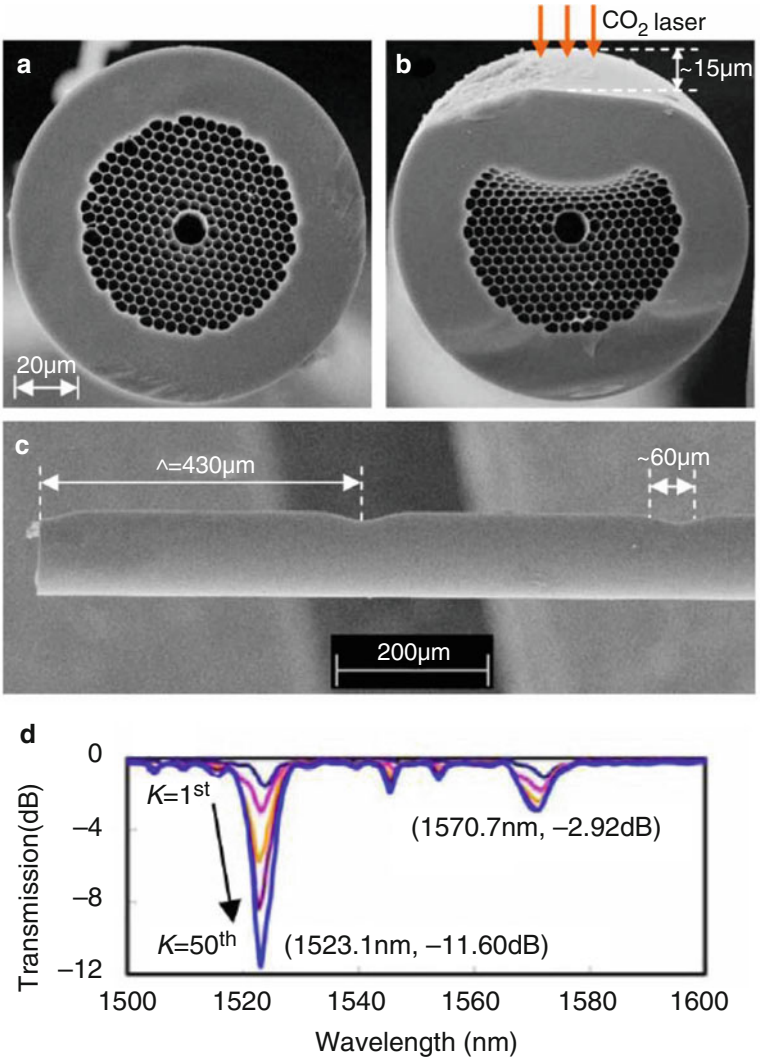

Fig. 30 SEM images of PBF cross sections (**a**) before and (**b**) after CO_2 laser irradiation. (**c**) Periodic notches on PBF after 50 scanning cycles. (**d**) Transmission spectrum of a 40-period LPG on PBF (Wang et al. 2008)

loss of the LPG is very low (<0.3 dB), because most light is guided in the hollow core where no deformation is observed.

Before the LPG is created, the light intensity is mainly in the fundamental mode, as shown in Fig. 31a. With an increase in the number of grating pitches, for the input light at 1523.1 nm, light energies near the core-cladding interface and in the holey cladding region are gradually enhanced whereas that in the fundamental mode is

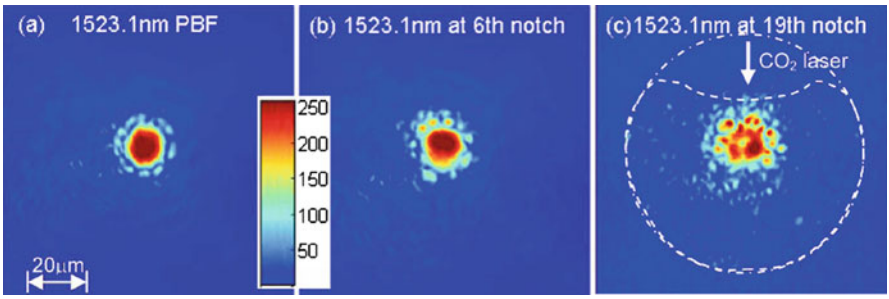

Fig. 31 (**a**) Near-field image in a PBF without LPG. (**b**) Near-field images of an LPG at the resonant wavelength of 1523.1 nm when the LPG is cut at 6th notch. (**c**) Near-field images of the same LPG observed at the 19th notch at 1523.1 nm (Wang et al. 2008)

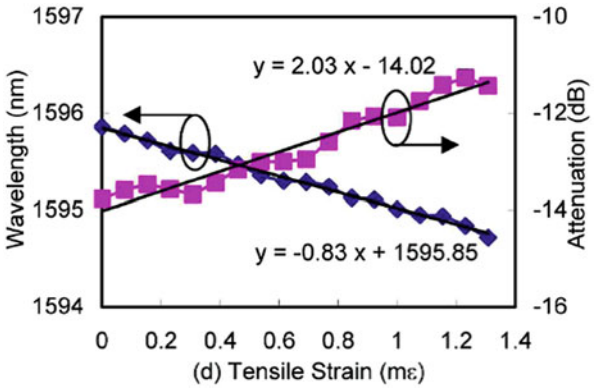

Fig. 32 Measured resonant wavelength and peak transmitted attenuation of the LPG versus tensile strain (Wang et al. 2008)

reduced, as shown in Fig. 31b, c. At the 19th notch, most energy in the fundamental mode is coupled out so that the light energies near the core-cladding interface and in the holey region are clearly observed and light intensity at the center of hollow core becomes very weak. Light coupled into the cladding region is mainly distributed within the holey cladding region as outlined by the dashed curve, and the energy in the side facing to CO_2 laser irradiation is stronger than that in the opposite side.

For the PBG-based LPG, the temperature sensitivity is ~2.9 pm/°C, which is one to two orders of magnitude less than those of the LPGs in SMFs. The curvature sensitivity is three to four orders of magnitude less than those of the LPGs in SMFs. With the increase of applied tensile strain, the resonant wavelength of the LPG is shifted linearly toward shorter wavelength with a strain sensitivity of −0.83 nm/mε, and the peak transmission attenuation is decreased with a sensitivity of 2.03 dB/mε, as shown in Fig. 32. The wavelength sensitivity to strain is two times higher than that of LPGs in SMFs, indicating that this LPG may be used as a strain sensor without cross-sensitivity to temperature and curvature.

Tensile Strain Sensing by Use of the LPG in All-Solid PBF

C. R. Liao et al. presented an LPG inscribed in all-solid PBF by use of femtosecond laser with line-scanning method (Liao et al. 2010). The employed PBF has an index-depressed layer (fluorine-doped) around the high-index rods (germanium-doped) in the unit cell of photonic crystal cladding, as shown in Fig. 33. The diameter of the fiber is 123 μm and the lattice spacing Λ is 9.21 μm. In the experiment, 5 cm of the PBF is spliced to SMF-28 fiber which are well aligned to restrain mode couplings between the high-index rods and the fiber core as well as to minimize the insertion loss.

LPGs are fabricated by use of an amplified 800-nm femtosecond laser system. The PBGF supports both LP_{01} and LP_{11} bandgap-guided core modes. At 1550 nm, n_{eff} of the fundamental mode (LP_{01}) and higher-order core mode (LP_{11}) are calculated to be 1.4419 and 1.4407 using finite element method. In order to satisfy phase-matching condition between the two core modes ~1550 nm, the period of the LPG is chosen as 640 μm, and the grating length is 24 mm. One piece of SMF-28 fiber was spliced onto the PBF to prevent the high-order core mode (LP_{11}) coupling from LP_{01}, and thus the LPG attenuation band can appear. Figure 34a shows the transmission spectrum evolution of the LPG within 38 periods. The resonance wavelength of the LPG created is located at 1542.3 nm, with a full-width at half-maximum (FWHM) value of ~24 nm, and the strongest resonance is measured as ~19 dB. Figure 34b, c illustrates the near-field images of the PBF at 1542.3 nm before and after the LPG inscription, respectively. Before the LPG is inscribed, the light intensity is mainly in the fundamental mode (LP_{01}) with a small part (super-modes) being distributed in the high-index rods, especially in the six rods being close to the core, as shown in Fig. 34b.

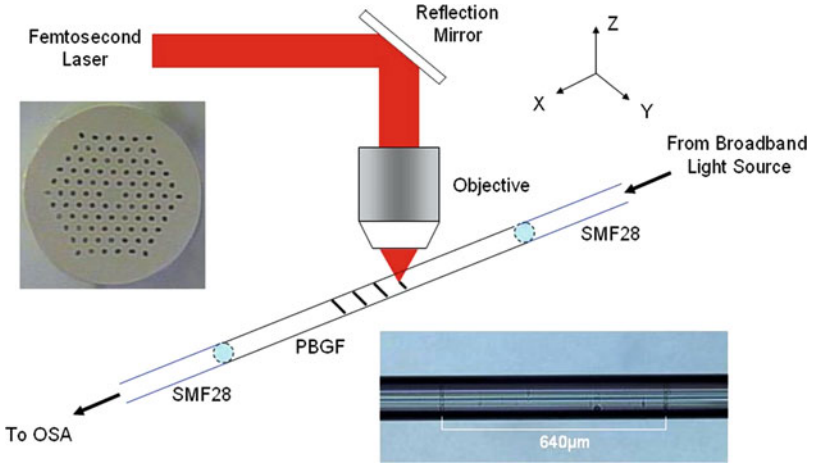

Fig. 33 Experimental setup for LPG fabrication by use of femtosecond laser with line-scanning method (Liao et al. 2010)

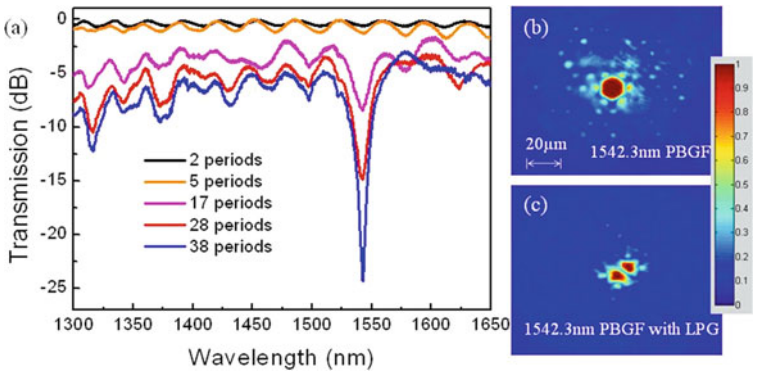

Fig. 34 (**a**) Evolution of the transmission spectrum of LPG with the increase of period number (2∼38), the grating pitch is 640 μm. (**b**) Near-field image in an all-solid PBF without LPG. (**c**) Near-field image at the resonant wavelength of 1542.3 nm with the period number of 38 (Liao et al. 2010)

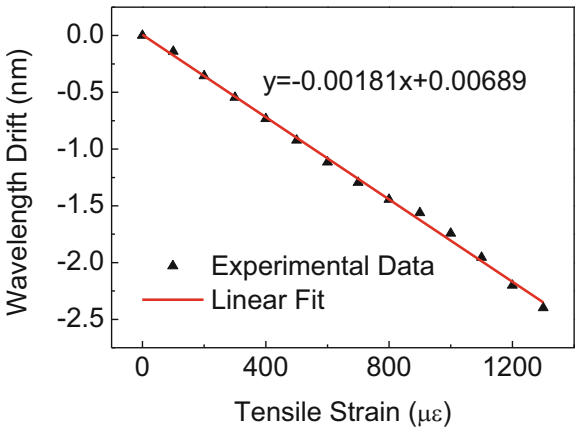

Fig. 35 Measured resonant wavelength of the LPG versus tensile strain (Liao et al. 2010)

Figure 35 demonstrates the response of the LPG to tensile strain. There is a linear "blue" shifting for the resonant wavelength with the increase of applied tensile strain. The measured sensitivity is −1.8 nm/mε, this being four times higher than those of LPGs in conventional SMFs.

Gas Pressure Sensing by Use of the LPG in Air-Core PBF

J. Tang et al. demonstrated an LPG inscribed in an air-core PBF for gas pressure sensing (Tang et al. 2015). The LPG is inscribed by use of CO_2 laser beam-scanning technique, which greatly enhanced the writing efficiency and repeatability, and the fabrication setup is shown in Fig. 36a. An air-core PBF (HC-1500-02 PBF from Crystal-Fiber) is employed to inscribe a LPG, as shown inset of Fig. 36a. Figure 36b shows the microscope image of the LPG with periodic collapse face to the CO_2 laser

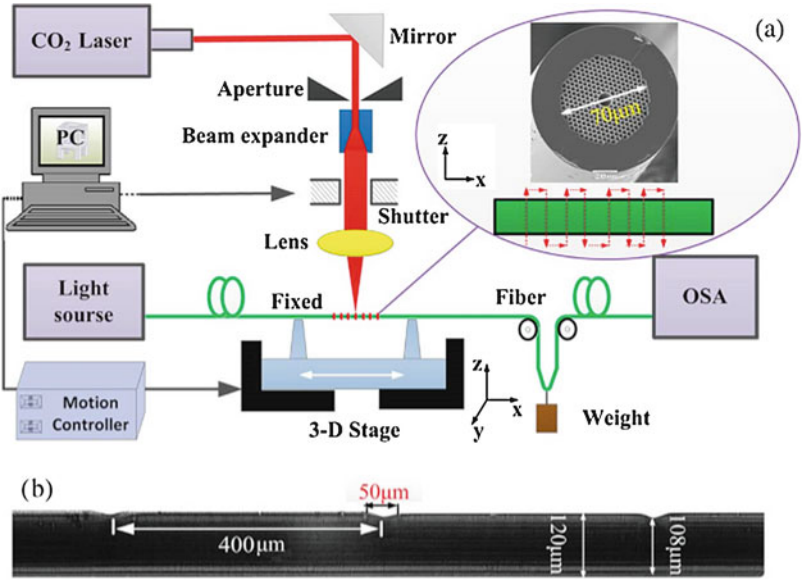

Fig. 36 (**a**) Experimental setup for LPG inscription with CO_2 laser beam-scanning technique. (Inset) SEM of the used HC-PBF. (**b**) Side view of the obtained LPG (Tang et al. 2015)

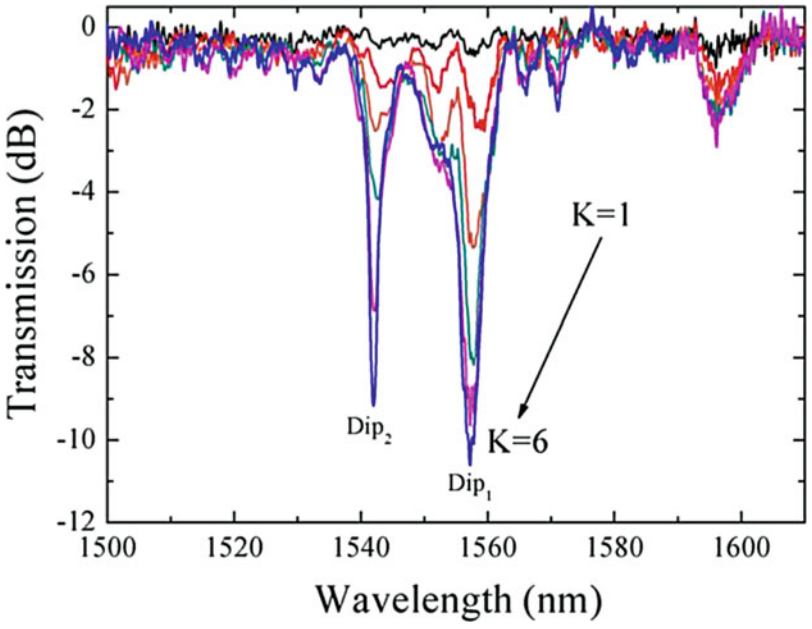

Fig. 37 Transmission spectral evolution of an LPG with grating pitch of 400 μm while the number of scanning cycles (K) increases from 1 to 6 (Tang et al. 2015)

exposure side. The width and depth of the collapsed region are 50 μm and 12 μm, respectively.

Figure 37 shows the transmission spectral evolution when the number of scanning cycles is increased from 1 to 6. Two resonant dips have been found at resonant wavelengths of 1555.9 nm (Dip1) and 1541.4 nm (Dip2), respectively. Two-step process might be involved: the fundamental core mode is coupled to discrete higher-order (core or surface-like) modes and then to lossy quasi-continuum of cladding and radiating modes. The depth of the two resonant dips gradually increases with an increase of scanning cycle and finally reached to −10.61 dB and −9.15 dB, respectively.

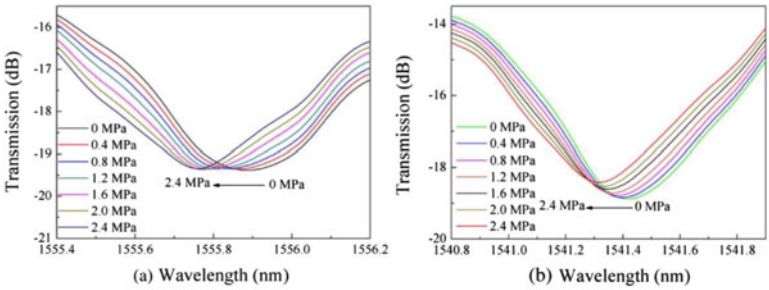

Fig. 38 Transmission spectrum evolution of (**a**) Dip1 and (**b**) Dip2 while the gas pressure increases from 0 to 2.4 MPa (Tang et al. 2015)

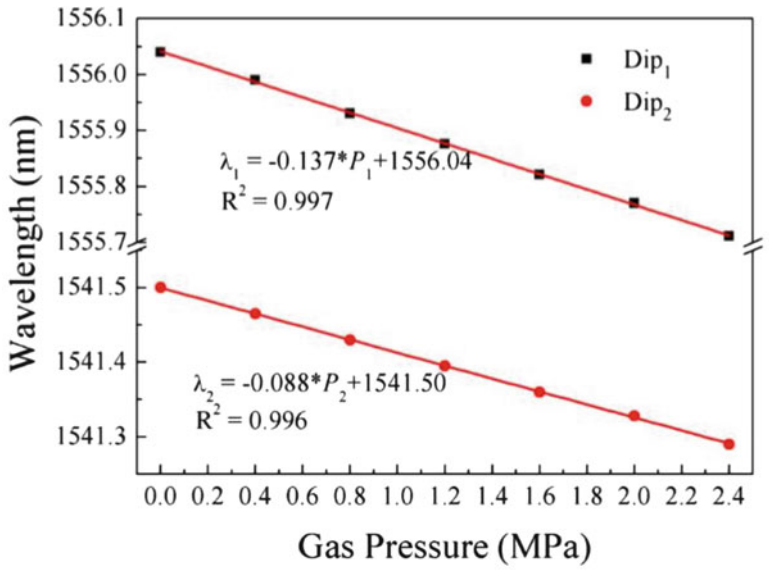

Fig. 39 Relationship between gas pressure and resonant wavelength of Dip1 and Dip2 while the gas pressure increases from 0 to 2.4 MPa (Tang et al. 2015)

The gas pressure responses of Dip1 and Dip2 are, respectively, monitored for better understanding pressure response of the LPGs written in the air-core PBF. As shown in Fig. 38a, b, both Dip1 and Dip2 shift toward shorter wavelengths with the pressure increasing gradually from 0 to 2.4 MPa with an interval of 0.4 MPa. The relationship between resonant wavelength and gas pressure is shown in Fig. 39. The experiment sensitivity of Dip1 and Dip2 are −137 pm/MPa and −88 pm/MPa, respectively. The PBF-based LPG exhibits a high-pressure sensitivity that is due to more significant physical deformation in air-core PBF.

References

B.J. Eggleton, P.S. Westbrook, R.S. Windeler, S. Spälter, T.A. Strasser, Grating resonances in air-silica microstructured optical fibers. Opt. Lett. **24**, 1460–1462 (1999)

L.B. Fu, G.D. Marshall, J.A. Bolger, P. Steinvurzel, E.C. Mägi, M.J. Mithford, B.J. Eggleton, Femtosecond laser writing Bragg gratings in pure silica photonic crystal fibres. Electron. Lett. **41** (2005)

T. Geernaert, G. Luyckx, E. Voet, T. Nasilowski, K. Chah, M. Becker, H. Bartelt, W. Urbanczyk, J. Wojcik, W.D. Waele, J. Degrieck, H. Terryn, F. Berghmans, H. Thienpont, Transversal load sensing with fiber Bragg gratings in microstructured optical fibers. IEEE Photon. Technol. Lett. **21**, 6–8 (2009)

Y.G. Han, Y.J. Lee, G.H. Kim, H.S. Cho, S.B. Lee, C.H. Jeong, C.H. Oh, H.J. Kang, Transmission characteristics of fiber Bragg gratings written in holey fibers corresponding to air-hole size and their application. IEEE Photon. Technol. Lett. **18**, 1783–1785 (2006)

M. Huy, G. Laffont, V. Dewynter, P. Ferfinand, L. Labonté, D. Pagnoux, P. Roy, W. Blanc, B. Dussardier, Tilted fiber Bragg grating photowritten in microstructured optical fiber for improved refractive index measurement. Opt. Express **14**, 10359–10370 (2006)

L. Jin, Z. Wang, Q. Fang, B. Liu, Y.G. Liu, G.Y. Kai, X.Y. Dong, B.O. Guan, Bragg grating resonances in all-solid bandgap fibers. Opt. Lett. **32**, 2717–2719 (2007)

L. Jin, W. Jin, J. Ju, Directional bend sensing with a CO_2 laser inscribed long period grating in a photonic crystal fiber. J. Lightwave Technol. **27**, 4884–4891 (2009)

J.C. Knight, T.A. Birks, P.S.J. Russell, D.M. Atkin, All-silica single-mode optical fiber with photonic crystal cladding. Opt. Lett. **21**, 1547–1549 (1996)

Y.H. Li, D.N. Wang, L. Jin, Single-mode grating reflection in all-solid photonic bandgap fibers inscribed by use of femtosecond laser pulse irradiation through a phase mask. Opt. Lett. **34**, 1264–1266 (2009)

C.R. Liao, Y. Wang, D.N. Wang, L. Jin, Femtosecond laser inscribed long-period gratings in all-solid photonic bandgap fibers. IEEE Photon. Technol. Lett. **22**, 425–427 (2010)

L. Rindorf, J.B. Jensen, M. Dufva, L.H. Pedersen, P.E. Hoiby, O. Bang, Photonic crystal fiber long-period gratings for biochemical sensing. Opt. Express **14**, 8224–8231 (2006)

J. Tang, G.L. Yin, S. Liu, X.Y. Zhong, C.R. Liao, Z.Y. Li, Q. Wang, J. Zhao, K.M. Yang, Y.P. Wang, Gas pressure sensor based on CO_2 laser induced long period fiber grating in air-core photonic bandgap fiber. IEEE Photon. J. **7**, 6803107 (2015)

Y.P. Wang, L.M. Xiao, D.N. Wang, W. Jin, Highly sensitive long-period fiber-grating strain sensor with low temperature sensitivity. Opt. Lett. **31**, 3414–3416 (2006)

Y.P. Wang, W. Jin, J. Ju, H.F. Xuan, H.L. Ho, L.M. Xiao, D.N. Wang, Long period gratings in air-core photonic bandgap fiber. Opt. Express **16**, 2784–2790 (2008)

P.S. Westbrook, B.J. Eggleton, R.S. Windeler, A. Hale, T.A. Strasser, G.L. Burdge, Cladding-mode resonances in hybrid polymer-silica microstructured optical fiber gratings. IEEE Photon. Technol. Lett. **12**, 495–497 (2000)

C. Wu, B.O. Guan, Z. Wang, X.H. Feng, Characterization of pressure response of Bragg gratings in grapefruit microstructured fibers. J. Lightwave Technol. **28**, 1392–1397 (2010)

X. Yu, P. Shum, G.B. Ren, Highly sensitive photonic crystal fiber-based refractive index sensing using mechanical long-period grating. IEEE Photon. Technol. Lett. **20**, 1688–1690 (2008)

X.Y. Zhong, Y.P. Wang, C.R. Liao, S. Liu, J. Tang, Q. Wang, Temperature-insensitive gas pressure sensor based on inflated long period fiber grating inscribed in photonic crystal fiber. Opt. Lett. **40**, 1791–1794 (2015)